






Article

Age and Depositional Environment of Whale-Bearing Sedimentary Succession from the Lower Pliocene of Tuscany (Italy): Insights from Palaeomagnetism, Calcareous Microfossils and Facies Analyses

Mattia Marini ¹, Luca Maria Foresi ^{2,*}, Viviana Barbagallo ³, Michelangelo Bisconti ^{4,5}, Agata Di Stefano ³, Giovanni Muttoni ¹ and Ivan Martini ²

¹ Dipartimento di Scienze della Terra 'Ardito Desio', Università di Milano, 20133 Milan, Italy

² Dipartimento di Scienze Fisiche, della Terra e dell'Ambiente, Università di Siena, 53100 Siena, Italy

³ Dipartimento di Scienze Biologiche Geologiche e Ambientali, Università di Catania, 95125 Catania, Italy

⁴ Dipartimento di Scienze della Terra, Università degli Studi di Torino, 10124 Torino, Italy

⁵ San Diego Natural History Museum, San Diego, CA 121390, USA

* Correspondence: luca.foresi@unisi.it

Abstract: A c. 31 m thick section straddling the fossil find of an Early Pliocene baleen whale ("Brunella", hereafter), made in 2007 in the sedimentary fill of the Middle Ombrone Basin of Tuscany, is investigated for depositional age and environment combining palaeomagnetic, micropalaeontological (Foraminifera and calcareous nannofossils) and sedimentary facies analyses. Resting unconformably onto Late Miocene continental deposits, the Early Pliocene marine deposits include, from bottom to top, a coarse-grained wave-winnowing lag, the few metres-thick fossiliferous sandstone bedset from which Brunella was unearthed, and several metres of clays. The stratigraphic organisation of these deposits indicate deposition in a deepening upward inner shelf environment. Successful isolation of characteristic remanent magnetisation and calcareous nannofossil content indicate the investigated marine section was deposited during the interval of polarity Chron C3n.2n corresponding to the basal part of the Mediterranean nannofossil zone MNN13 (between *Helicosphaera sellii* Base common and the *Amaurolithus primus* Top) and allow estimating the depositional age of Brunella to c. 4.6 Ma. Sedimentary facies, benthic Foraminifera association and anisotropy of magnetic susceptibility characterising the deposits that embedded Brunella suggest deposition above the fair-weather base level.

Keywords: fossil whale; Italy; Tuscany; Pliocene; depositional environment; sedimentary facies analyses; magnetostratigraphy; calcareous plankton biostratigraphy



Citation: Marini, M.; Foresi, L.M.; Barbagallo, V.; Bisconti, M.; Di Stefano, A.; Muttoni, G.; Martini, I. Age and Depositional Environment of Whale-Bearing Sedimentary Succession from the Lower Pliocene of Tuscany (Italy): Insights from Palaeomagnetism, Calcareous Microfossils and Facies Analyses. *J. Mar. Sci. Eng.* **2023**, *11*, 455. <https://doi.org/10.3390/jmse11020455>

Academic Editor: Dimitris Sakellariou

Received: 15 December 2022

Revised: 1 February 2023

Accepted: 14 February 2023

Published: 19 February 2023



Copyright: © 2023 by the authors. Licensee MDPI, Basel, Switzerland. This article is an open access article distributed under the terms and conditions of the Creative Commons Attribution (CC BY) license (<https://creativecommons.org/licenses/by/4.0/>).

1. Introduction

Pliocene deposit outcrops in Tuscany (central Italy) contain a relatively rich fossil record of marine megafauna (Figure 1; see [1] for an extensive review) that appears significantly different from that of the latest Miocene [2,3], predating the Messinian Salinity Crisis [4]. Particularly, several palaeontological works have shown that there is a major discontinuity between the Late Miocene and the Pliocene mysticete faunas at a global scale [5,6]. In the fossil Balaenidae record of Tuscany, this Early Pliocene event is largely documented [7,8] and characterised by a relative increase in balaenid and balaenopterid diversity (Event 3 in [5]). However, very little is known about the first mysticetes that re-invaded the Mediterranean as normal salinity conditions were re-established in the Early Pliocene. Therefore, better understanding of taxonomy and age of fossil mysticetes from the Zanclean stage is key to establish robust phylogenetic relationships, palaeobiogeography and, ultimately, ecologic and trophic webs of these marine mammals [9–13].

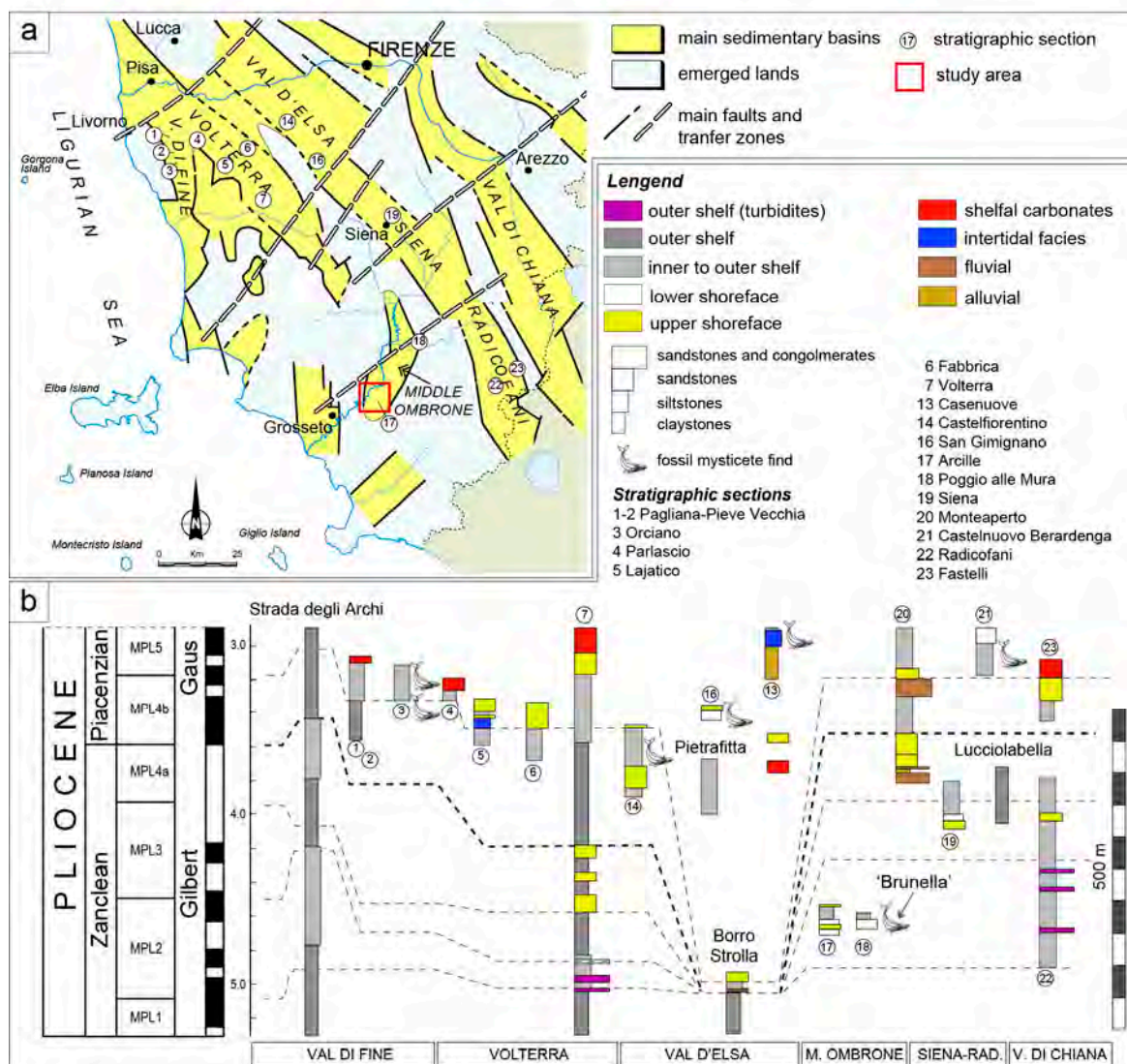


Figure 1. (a) Simplified geological sketch showing the Plio-Quaternary basins of Tuscany (modified, after [14]). (b) Stratigraphic scheme based on biostratigraphic correlation of selected sections (see geological sketch for location and legend for section names) from the marine Pliocene of Tuscany (modified, after [1]) with occurrence of fossil mysticetes from [1].

This study focuses on the integrated stratigraphy (magnetostratigraphy, biostratigraphy and sedimentary facies analyses) of a sedimentary section (Brunella composite section, hereafter) exposed near Montalcino (c. 42 km SE of Siena; Figure 1a) and straddling the site where a partial skeleton of a mysticete balaenopterid was discovered in 2007 [15,16].

The specimen (ICCD 09 0000001-18; Figure 2), currently under investigation for taxonomy, was nicknamed Brunella and rapidly gained some research interest for its supposed Zanclean age (Figure 1b), which makes it one of the rare records of Early Pliocene mysticetes of Tuscany [16]. The aim of the study is twofold: (i) dating the sedimentary succession embedding Brunella by combining magnetostratigraphy and calcareous plankton biostratigraphy (planktonic Foraminifera and calcareous nannofossils) and (ii) providing a depositional model for the Brunella composite section based on sedimentary facies analysis, benthic Foraminifera ecology and anisotropy of magnetic susceptibility (AMS, hereafter).

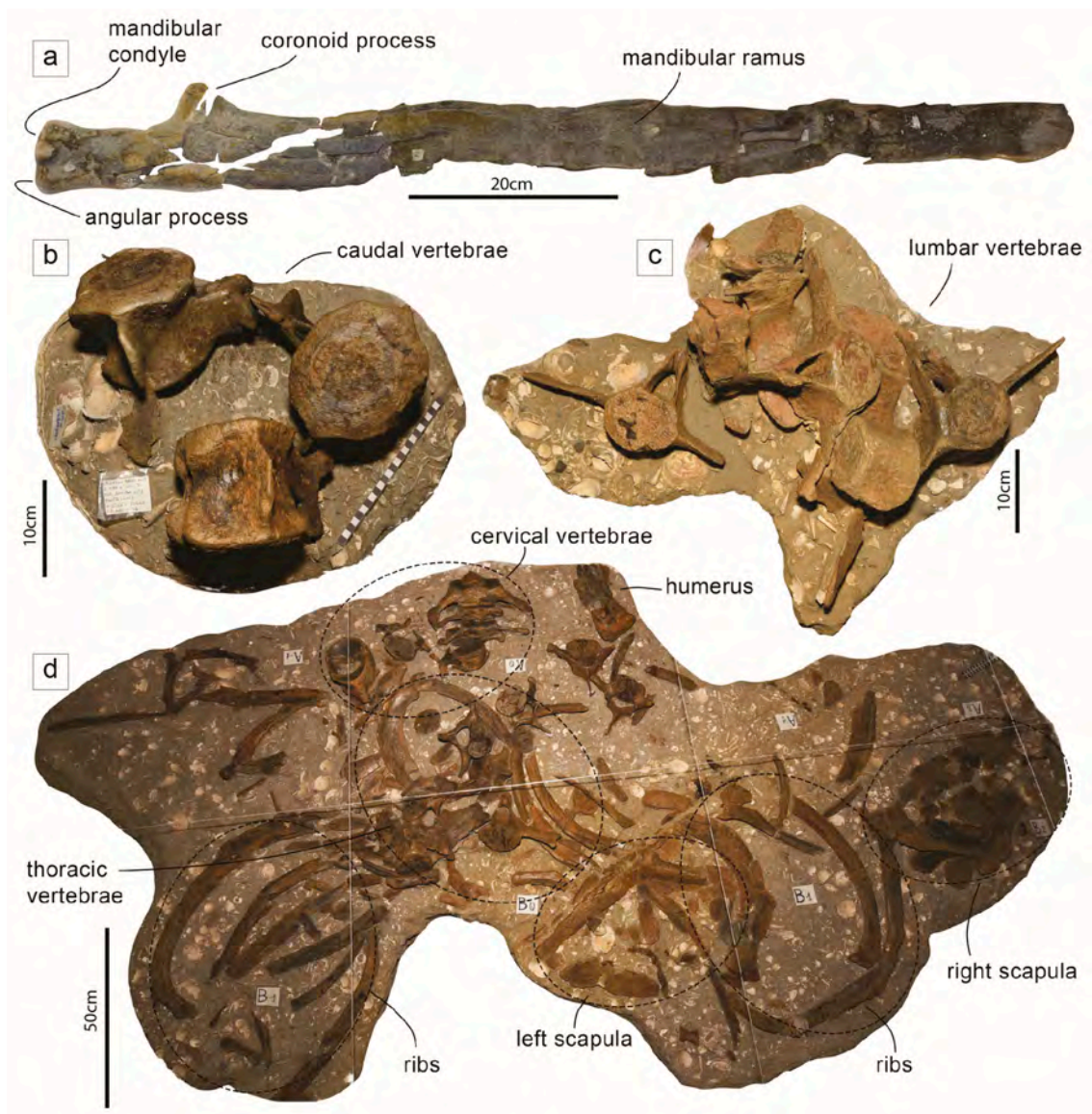


Figure 2. Skeletal portions of the ICCD 09 00000001-18 whale nicknamed Brunella. (a) Left dentary showing typical balaenopterid characters in the posteriorly-oriented mandibular condyle, reduced angular process and comparatively long distance between the condyle and the coronoid process; (b) group including caudal vertebrae 3 to 5; (c) group including disarticulated lumbar vertebrae; (d) large block including cervical and thoracic vertebrae, two scapulae, one humerus and most of the ribs.

2. Geological Setting

The investigated sedimentary succession (Figure 3) is part of the sedimentary fill of the Middle Ombrone Basin of Tuscany ([17–19]; cf. with the Cinigiano–Baccinello Basin of [20]), one of several continental to marine Plio-Quaternary basins (Figure 1a) formed since the late Neogene as a result of crustal extension in the Apennine hinterland [17,21–25]. These late orogenic basins are regarded as graben-like elongated depocentres striking parallel to the central Apennine chain that were infilled relatively rapidly by continental and shallow marine clastics [23,26]. Even though a purely extensional horst-and-graben model is supported by the lack of significant tectonic rotation since the late Messinian [27], other authors suggested that late orogenic basins of Tuscany may have formed in a more complex tectonic setting, in which compressional, extensional and strike-slip stress regimes coexisted and/or alternated over time [28,29]. Recently, other studies suggested that these basins

developed as hanging-wall basins associated with extensional detachments (Serravallian–late Messinian) that formed a bowl-shaped structural depressions later dissected by late Zanclean–early Piacenzian high-angle normal faults [25,30,31].

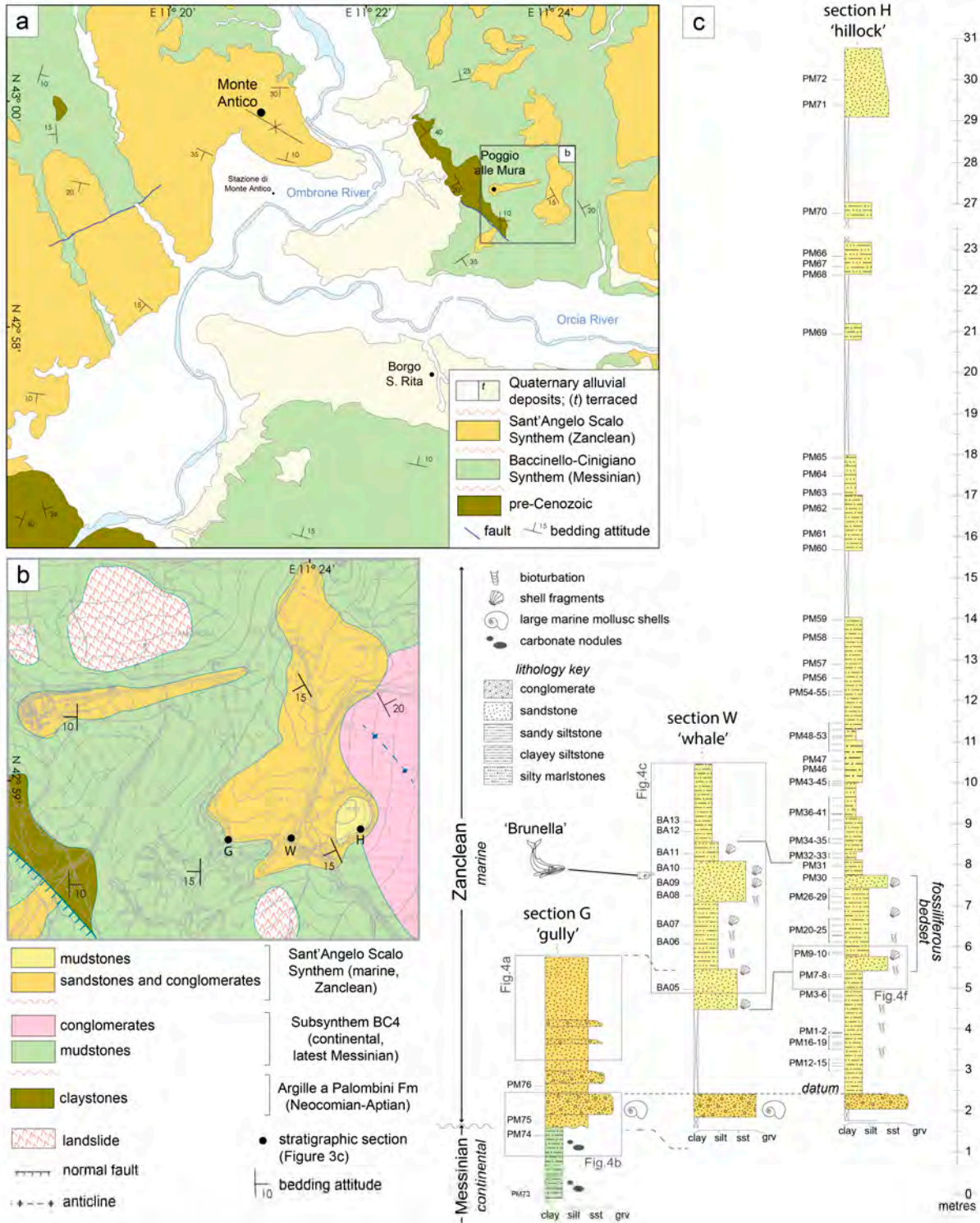


Figure 3. (a) Simplified geological map and (b) detail of the study area (modified, after [20,32]) with location of the sections making the Brunella composite section; (c) stratigraphic log of the Brunella composite section with positions of samples. Section G 'gully' (Figure 4).



Figure 4. (a) The amalgamated bedset of marine sandstones (sst) and conglomerates (cgl) of section G. This bedset is erosion-based (b) and sits on top of plane-parallel laminated mudstones devoid of marine fossils, most likely deposited in a continental flood-plain environment. (c) View of section W with detail, showing the top of the fossiliferous sandstone bedset from which *Brunella* was unearthed, sharply capped by mudstones; (d) view of the easterly outcrop with location of section H. (e) View of the lower part of section H with sites of palaeomagnetism sampling; (f) detail of the highly bioturbated basal part of the fossiliferous bedset. Arrows highlighting mollusc shell fragments (sf) and trace fossils (tf).

The Whale Brunella and Its Host Sedimentary Rocks

The notoriety of the investigated sedimentary section (Figure 3) is due to the find of *Brunella* (Figure 2) and the accompanying macrofossil biota [33,34], which is relatively rich and comprises molluscs, barnacles, shark teeth, fish otoliths, echinoids and wood fragments. Within a few months from its finding, *Brunella* was fully excavated, removed

from the field along with its silty sandstone matrix and stored in a warehouse of the wine company Banfi s.r.l. attached to the Poggio alle Mura medieval castle. In 2016, the Tuscan Archaeological Superintendency started a project [15,35] that is still ongoing and includes the study of several aspects of Brunella (e.g., musealisation, taxonomy, taphonomy, etc.)

Regarding the age of the sedimentary rocks embedding Brunella, early geological mapping placed them in the Lower Pliocene Argille Azzurre Auct. [36]. Subsequent geological mapping highlighted the site is located immediately above the boundary between the Upper Miocene (Baccinello–Cinigiano Synthem of [32]; cf. with CB1 of [20]) and the Lower Pliocene (cf. with S. Angelo Scalo Synthem of [32]; Figure 3a,b). Based on correlation with nearby sections, Ref. [1] attributed the upper and easterly part of the investigated stratigraphy (cf. with Poggio alle Mura section of [37]) to the planktonic foraminiferal Biozone MPL2 of [38], which is early Zanclean in age (between c. 5 and 4.5 Ma, following [39]).

Particularly, Ref. [1] interpreted the shell-rich bed containing Brunella as a marker fossiliferous layer (the *Haustator* shell bed of [1]) correlatable with that of the nearby sections of Arcille, Monte Antico and Camigliano [37,40,41] and suggested that the rapid transition to clayey shelf mudstones above represented a major transgressive surface. More recently, [42] studied the molluscan benthic assemblages of the Poggio alle Mura section highlighting a well-diversified community typical of intertidal and shallow subtidal settings of Early Pliocene age.

3. Materials and Methods

The c. 31 m thick Brunella composite section was obtained by logging two ancillary sections ('gully' and 'hillock' sections, respectively; labelled G and H in Figure 3b,c) to the west and to the east of the section where Brunella was unearthed ('whale' section, labelled W in Figure 3b,c) and correlating them walking out the whale-bearing fossiliferous bedset. Sections were logged using a high-precision Jacob staff with rotatable laser and graphical logs drawn in the field at a scale 1:100, taking note of lithology, grain size of the clastic component and fossiliferous content, including trace fossils.

Seventy-two oriented standard (10 cc) samples for palaeomagnetism were collected from section H (corresponding to the Poggio alle Mura section of [37]; Figure 3c) using a water-cooled electric drill. Rock magnetic and magnetostratigraphic analyses were performed at the Laboratory of Magnetostratigraphy and Palaeogeography (PalMag) of the University of Milan (Segrate, Milan). A sub-set of 4 samples was analysed for hysteresis loops and backfield isothermal remanent magnetisation acquisition (backfield IRM), using a Microsense EZ7 Vibrating Sample Magnetometer (VSM). Thermal demagnetisation of a three-component IRM [43] was performed on 8 samples exposed to 1.5 T, 0.4 T and 0.15 T orthogonal fields with an ASC IM-10-30 pulse magnetiser. Samples for natural remanent magnetisation (NRM) and IRM analyses were thermally demagnetised from room temperature up to a maximum of 685 °C in steps of 25 to 50 °C with an ASC TD48 furnace. The magnetic remanence was measured after each demagnetisation step with a 2G Enterprises 755 DC-SQUID (Direct Current—Superconducting Quantum Interference Device) cryogenic magnetometer hosted in a magnetically shielded room. The component directions of the characteristic remanent magnetisation (ChRM) were extracted with standard least-square analysis on linear portions of standard vector end-point demagnetisation diagrams.

Mean directions were calculated with standard Fisher statistics. The anisotropy of magnetic susceptibility (AMS, hereafter; [44]) of selected samples was measured at the Palaeomagnetism Laboratory of Roma TRE University (Italy) using a AGICO KLY-3 Kappabridge susceptibility meter. AMS is represented by three symmetrical tensors, representing as many susceptibility axes (k_1 , k_2 and k_3 in descending order of susceptibility) of an ellipsoid with variable shape and associated anisotropy. AMS is evaluated using Flinn and Jelinek scatterplots, in which the foliation $F = k_2/k_3$ is plotted against the lineation $L = k_1/k_2$, and the degree of magnetic anisotropy $P = k_1/k_3$ is plotted against the shape parameter $T = (\ln L/\ln F)/(\ln L + \ln F)$, respectively. Values of $F/L < 1$ for $0 < T < 1$ indicate oblate ellipsoids (i.e., disc-shaped), whereas values of $F/L > 1$ indicate prolate ellipsoids

(i.e., cigar shaped). In sediments, mean susceptibility $k_{\text{mean}} = (k_1 + k_2)/3$ and P are generally less than c. 300×10^{-6} and c. 1.05, respectively, and the anisotropy can be viewed as an oblate ellipsoid displaying imbrication angles up to c. 20° [44,45]. On the other hand, prolate ellipsoids with relatively higher k_{mean} [46] generally relate to tectonic deformation.

Samples for micropalaeontological analyses were collected at each site of palaeomagnetic sampling along section H and at several additional sites along sections G and W (Figure 3c) for a total of 85 samples. Based on abundance of the biogenic fraction in the washing residue, fifty samples were considered for semi-quantitative analyses of Foraminifera. Samples were dried under an infrared lamp, and 100 g of dried sediment was disaggregated in a 30% aqueous solution of 30 volume hydrogen peroxide for about six hours. The mixture was then washed through a 63 μm sieve using a water shower and the residue was dried under the infrared lamps prior to being sieved again through a 250 μm sieve. The two resulting fractions (i.e., smaller and larger than 250 μm) were observed under the microscope separately. Abundant washing residue was analysed to detect even the rarest species, particularly planktonic Foraminifera. On the other hand, smear-slides for the analysis of calcareous nannofossils were prepared following standard procedures. A small fraction of sediment was scratched from a fresh sample surface and mixed with a few drops of distilled water to obtain a mixture that was then smeared on a coverglass using a short plastic straw until banded areas of variable grain density material were obtained. The coverglass was then dried on a hotplate, glued to glass slide using a UV-curing optical adhesive and then placed below a UV lamp until completely dry. The smear-slides were analysed using a light microscope and a magnification of about $1000\times$.

4. Results

4.1. Sedimentary Facies Association

The basal part of the Brunella composite section (section G in Figure 3c) is exposed in a gully (Figure 4a). It begins with several metres of plane-parallel laminated mudstones (Figure 4b) devoid of marine fossils and with sparse carbonate nodules suggestive of deposition in a continental setting (cf. with the late Messinian unit CB1e of [20]). Carbonate nodules can be interpreted as pedogenic hydromorphic features (gleying) linked to ground-water table oscillations [47], a condition typical of poorly drained floodplains [48]. Above, the succession continues with a c. 3 m thick erosion-based bedset of sandstones and conglomerates (Figure 4a,b) containing fragments of large marine mollusc shells. These deposits are generally well-sorted, structureless and organised to form several tens of cm thick coarsening-upward sequences with grain size ranging from medium sand to large pebbles. The bedset is initiated by a c. 30 cm thick normally graded very coarse-grained sandstone with scattered pebbles and shell fragments and, overall, shows similarity with wave-winnowing lags described elsewhere developing across wave-ravinement surfaces [49–52]. This relatively coarse bedset can be followed laterally for several tens of metres toward the E before it is lost in the cover.

The first c. 2.5 m of section W are poorly exposed but include a conglomerate made of well-sorted medium/large pebbles, locally with a coarse sandy matrix, which, based on similar character, was correlated to the lowermost conglomerate beds of section G (Figure 3c). Pebbles are well-rounded and commonly encrusted by barnacles and serpulids. These deposits include relatively large fragments of robust shells of marine gastropods and bivalves. Above the poorly exposed interval, the section continues with a c. 4 m thick fossiliferous sandstone bedset rich in shell fragments and bioturbated. From base to top, the bedset includes a c. 1 m thick fine-grained sandstone, 1.7 m of sandy siltstones and the 1 m thick medium-grained pebbly sandstone in which the disarticulated, partial skeleton of Brunella was found (Figure 4c). The top surface of the fossiliferous bedset is slightly erosional and rippled and is overlain by a fining-upward sandy to clayey siltstone c. 2.5 m thick (Figure 4c).

The fossiliferous bedset of section W can be followed laterally for several tens of metres toward the east, before it disappears in the cover in the close vicinity of section H.

Its stratigraphic position suggests it corresponds to a relatively finer-grained c. 2 m-thick bedset of section H, comprised of two sandstone beds sandwiching a sandy siltstone (Figures 3c and 4e,d). This correlation is confirmed by the occurrence of a at the base of section H, which after flattening the two section to the top of the fossiliferous bedset, turns out to be at the same stratigraphic level as the conglomerate at the base of section W. As a result, the fossiliferous bedset thins toward the E (from section W to section H) by c. 2 m over a distance of c. 200 m.

Also in section H, the fossiliferous bedset is sharply overlain by clayey siltstones that alternates with relatively thinner intercalations of silty marlstones for c. 6 m, before the section is lost in the cover. Individual couplets of silty marlstone and the clayey siltstones, typically a few metres thick, can be viewed as coarsening upward parasequence-like packages (*sensu* [53]; cf. with 'all offshore' parasequences of [54]). The remaining part of the section is poorly exposed, but spot outcrops suggest a gradual increase in grain size before reaching the sandstone bed exposed at the top of the hillock.

4.2. Palaeomagnetism

4.2.1. Rock Magnetism

Backfield IRM acquisitions highlight that the remanent magnetisation is acquired in a stepwise manner and that, for most samples, saturation is not achieved at the maximum applied field of 2 T (Figure 5a). The coercivity of remanence H_{cr} varies in the range 0.05–0.2 T, suggesting co-existence of relatively low-coercivity ferromagnetic s.l. phases (e.g., magnetite or possibly iron sulphides) and high-coercivity (non-saturating) phases (e.g., hematite).

Hysteresis loops, corrected for the contribution of paramagnetic (positive slope) minerals, are relatively slender in the central section and tend to open up at higher fields (Figure 5b). Such wasp-waisted loop shapes [55,56] suggest the occurrence of magnetic phases with contrasting coercivities, in agreement with backfield IRM experiments. The ratios of saturation remanence to saturation magnetisation (M_{rs}/M_s) plotted against the ratios of coercivity of remanence to coercivity (H_{cr}/H_c) according to [57], with later modifications by [58,59], indicate that all of the analysed samples are characterised by values incompatible with single domain-multidomain magnetite mixtures and significant contents of greigite (Figure 5d).

Thermal demagnetisation of three-axis IRM suggests that the contribution to magnetisation of low-coercivity minerals (0.15 T curve in Figure 5c) is greater than that of intermediate and high coercivity minerals (0.4 and 1.5 T curves in Figure 5c). All thermal demagnetisation curves show a relatively gradual decay of magnetisation, punctuated by inflections. The 0.15 T curves show inflections centred around 300 °C, before reaching complete demagnetisation at c. 580 °C (Figure 5c). On the other hand, the 0.4 T and 1.5 T curves show maximum unblocking temperatures of c. 675 °C (Figure 5c). All in all, results of rock magnetic experiments are suggestive of a complex magnetic mineralogy, most likely comprising magnetite, hematite and iron sulphides.

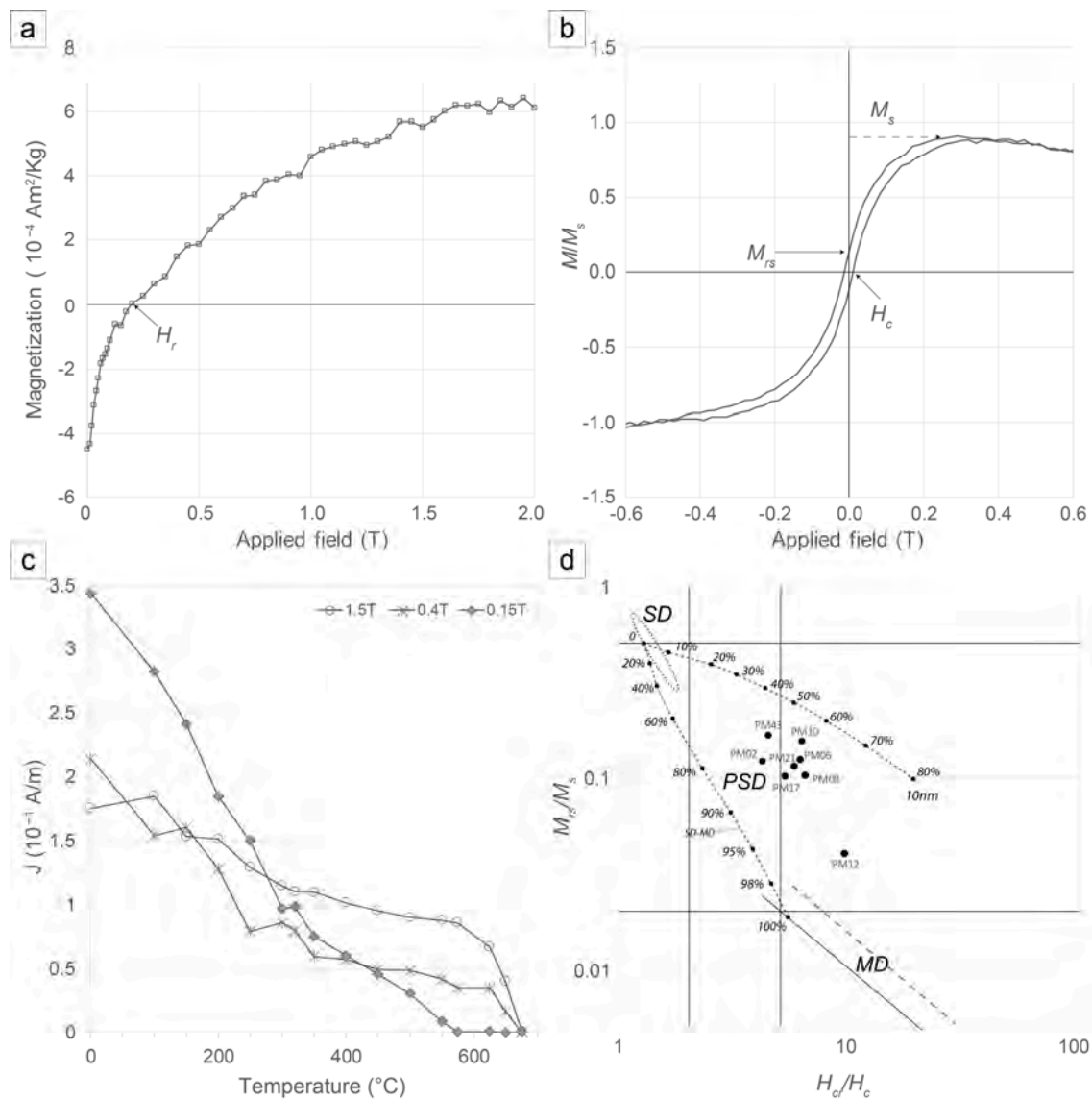


Figure 5. (a) IRM backfield acquisition curve, (c) hysteresis loop and (b) thermal demagnetisation paths of three-axes IRM of the representative sample PM06 (see Figure 3c for stratigraphic position); (d) Log–log scatter plot of ratio of saturation remanence to saturation magnetisation (M_{rs}/M_s) against ratio of remanent coercive force to ordinary coercive force (H_{cr}/H_c) of all samples analysed for magnetic carrier mineralogy. Black lines delimit variability fields of single domain (SD), pseudo-single domain (PSD) and multidomain (MD) grains after [57]. Dotted lines are theoretical mixing curves of SD+MD (below) and superparamagnetic (SP)+SD magnetites after [58]. The ellipse in the upper left corner highlights values of greigite-bearing samples from a global compilation by [59].

4.2.2. Characteristic Remnant Magnetisation

Reliable ChRM directions were isolated for 60 samples by selectively removing a secondary component between room temperature and 150 °C. ChRM directions are relatively stable across an unblocking temperature that is typically in the range 150–300 °C, but can extend up to 650 °C (e.g., PM15 and PM31, and PM50 and PM43, respectively; Figure 6).

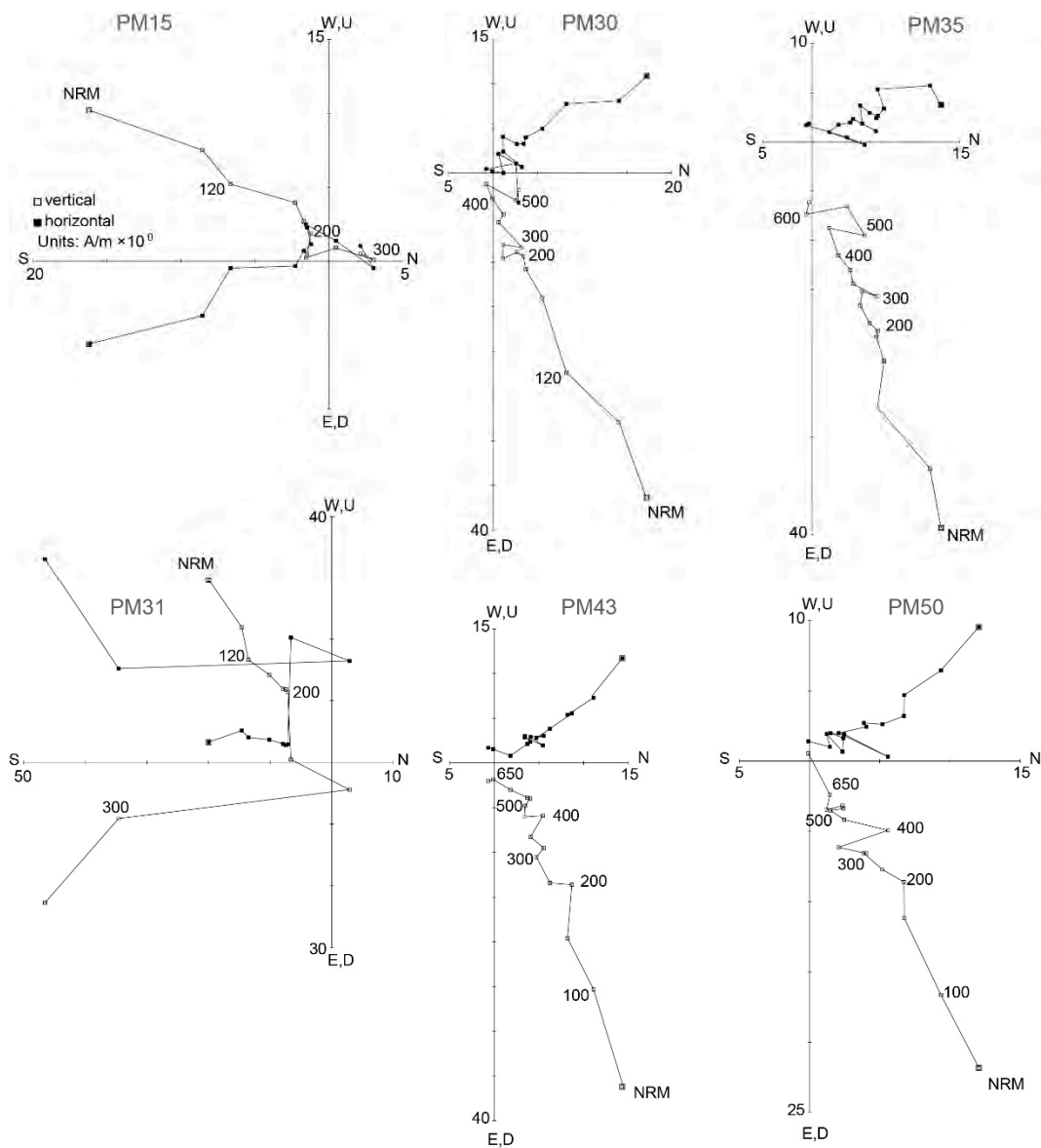


Figure 6. Vector end-point demagnetisation diagrams for representative samples (see Figure 3c for stratigraphic position) in in situ coordinates. Closed (open) squares are projections onto the horizontal (vertical) plane.

They are associated to mean angular deviation (MAD) values generally $<10^\circ$ (Figure 7) and appear oriented to the north and down (positive inclinations, e.g., PM30 in Figure 6) in all samples, with the exception of samples PM15 and PM31 (Figure 6), which are oriented to the south and up (negative inclinations). These ChRM component directions are grouped around an overall mean direction of Dec = 353.1° E, Inc = 57.9° ($k = 17.4$, $\alpha_{95} = 4.5$, $n = 60$) in in situ (geographic) coordinates, and of Dec = 328.7° E, Inc = 58.3° after correction for homoclinal bedding tilt (Figure 8 and Table 1).

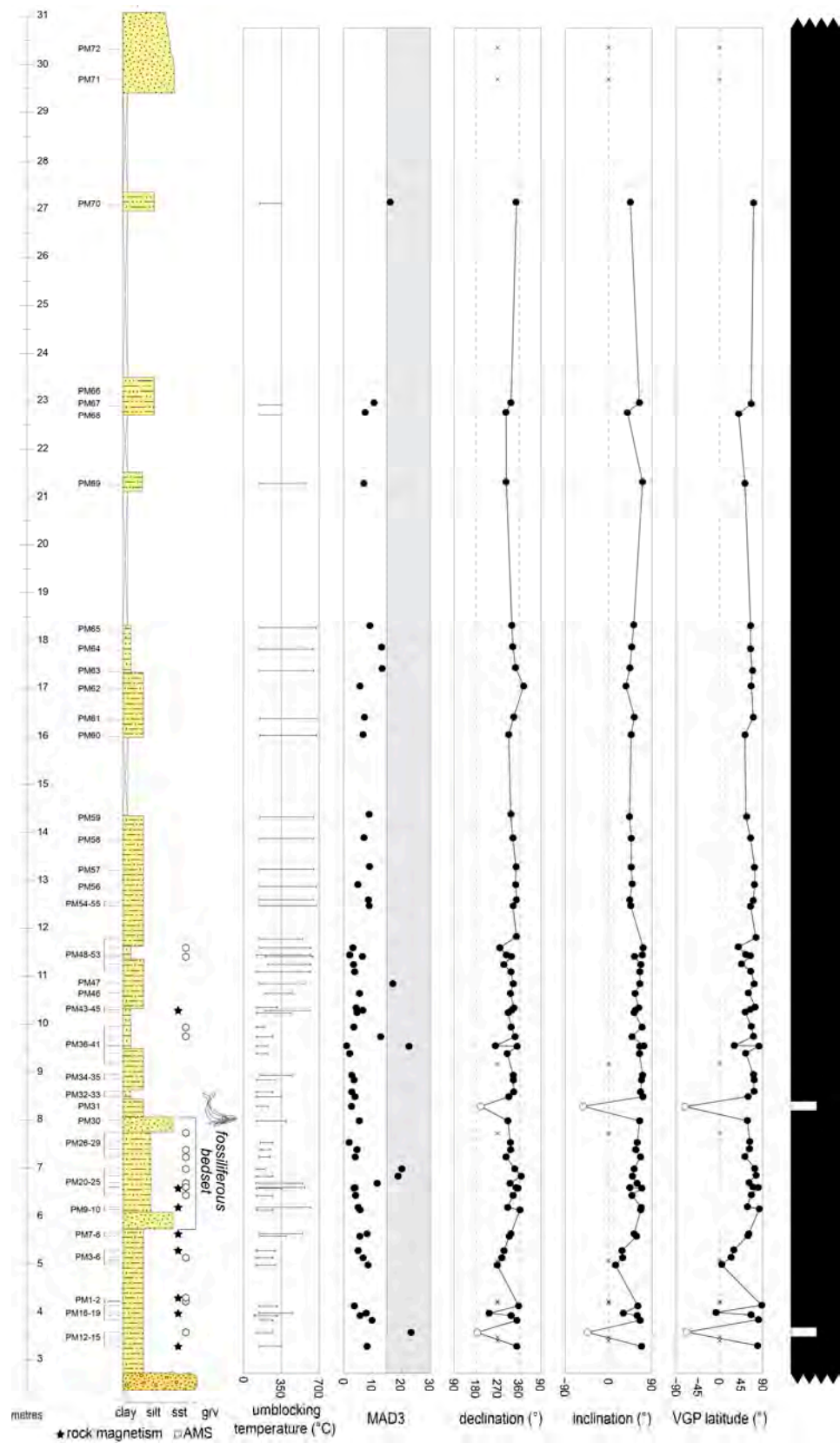


Figure 7. Stratigraphic log of section H (see Figure 3b,c for location and stratigraphic position, respectively) with (from left to right, unblocking temperature of ChRM, mean angular deviation (MAD), declination, inclination and virtual geomagnetic pole (VGP) and interpreted magnetic polarity.

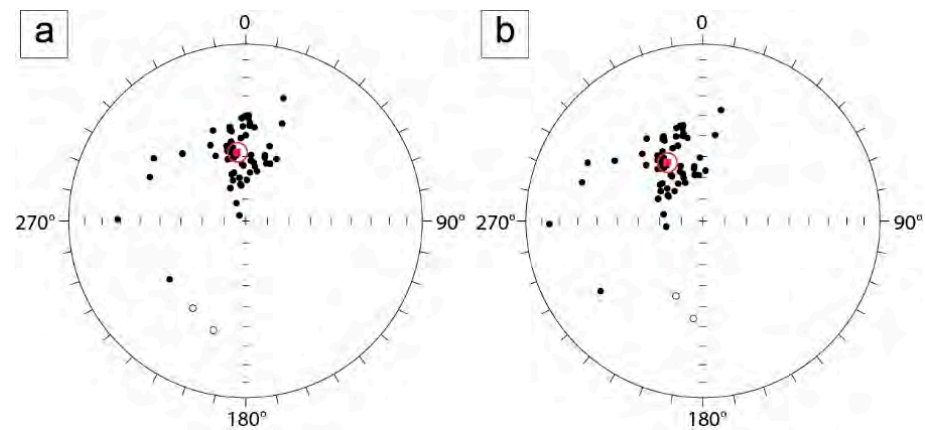


Figure 8. Equal-area projections of the ChRM component directions from palaeomagnetic samples from section H in (a) in situ (geographic) and (b) tilt-corrected coordinates. In red, mean direction (square) with a95 confidence.

Table 1. Palaeomagnetic mean directions from samples collected along section H (Figure 7). N: number of samples; k: Fisher precision parameter; a95: radius of the cone of 95% confidence; Dec.: mean Declination of the ChRM component; Inc.: mean Inclination of the ChRM component.

Mean Directions								
N	k	In Situ			k	Tilt-Corrected		
		a95	Dec.	Inc.		a95	Dec.	Inc.
60	17.4	4.5°	353.1°E	57.9°	17.4	4.5°	328.7°	58.3°

The tilt-corrected direction indicates a counter-clockwise tectonic rotation of c. 31°, which is slightly greater than that reported from some sites of similar age located in other Neogene basins of Tuscany (cf. with sites TS14 and TS05 from the Volterra Basin and TS01 and TS10 from the Siena–Radicofani Basin in [27]).

The declination and inclination values of the ChRM component directions and the associated virtual geomagnetic pole (VGP) latitudes plotted versus stratigraphic thickness show the occurrence across the sampled section of an at least c. 25 m thick interval of normal magnetic polarity (positive VGP values), interrupted by two intervals of single-sample reverse polarity (negative VGP values) (Figure 7).

4.2.3. Anisotropy of Magnetic Susceptibility (AMS)

Samples analysed for AMS come from the sedimentary package of Section H straddling the bed of Section W where Brunella was found, are relatively sandy and, in some instances, rich in mm-sized shell fragments. Mean susceptibility k_{mean} and anisotropy degree P are in the ranges $0.6\text{--}2 \times 10^{-4}$ and 1–1.057 (Figure 9a,b) and are largely uncorrelated (Figure 9b), albeit there is the tendency of stratigraphically higher and finer-grained samples to show larger values of both k_{mean} and P. This may relate to a relative increase in amount of paramagnetic minerals, such as micas. Scrutiny of Flinn and Jelinek scatterplots (Figure 9c,d) indicates that all samples are characterised by oblate AMS ellipsoids, which coupled with relatively low values of k_{mean} and P, suggests the AMS fabric is of sedimentary origin.

However, there is no clear clustering of the k_3 axes perpendicular to bedding planes, as expected in sedimentary rocks deposited in low-energy environments [60]. This may reflect superimposition of different factors, including continuous sediment reworking by wave action and, secondarily, modification of primary fabric by bioturbation.

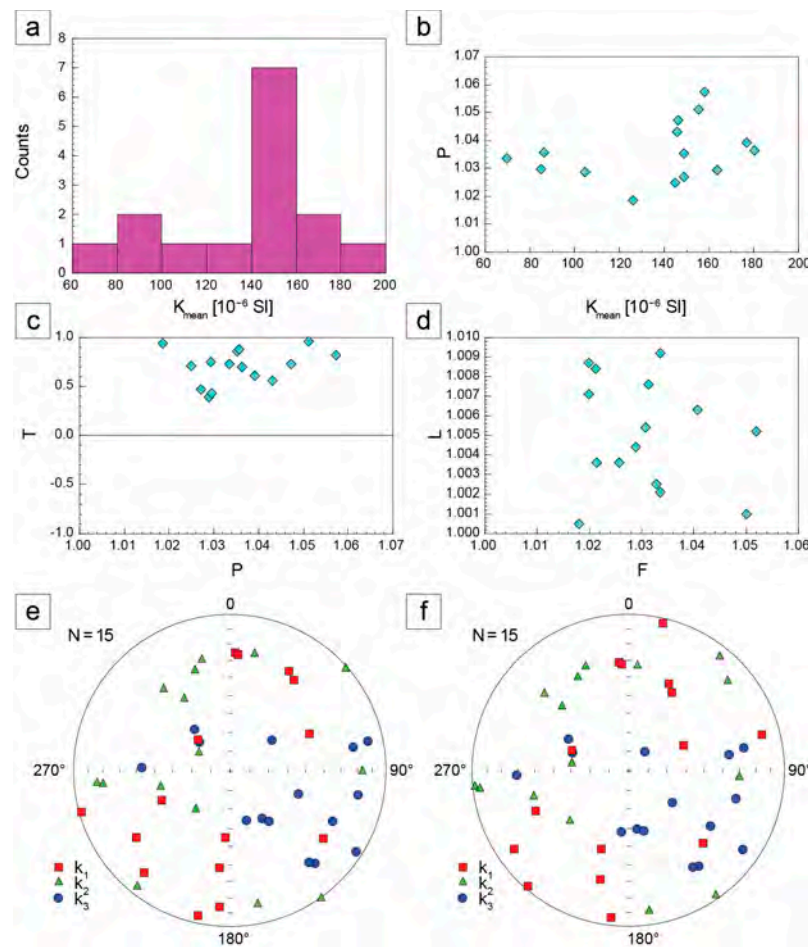


Figure 9. Anisotropy of Magnetic Susceptibility (AMS) of selected samples from the whale-bearing layer in section H (see Figure 3 for stratigraphic position). (a) Histogram of k_{mean} . (b) Scatterplot of shape parameter P to k_{mean} suggesting there is no correlation between AMS shape and susceptibility intensity. (c) Jelinek and (d) Flinn scatterplots highlighting the prolate nature of AMS ellipsoids. (e) In situ and (f) tilt-corrected equal area projection of poles of k_1 , k_2 and k_3 susceptibility axes.

4.3. Micropalaeontology

4.3.1. Calcareous Plankton

The calcareous plankton assemblages of the Brunella composite section comprise both nannofossils and Foraminifera that, although generally rare, provide useful biostratigraphic insights (see Section 5.1).

Abundance and preservation of calcareous nannofossil assemblages range from scarce to common and from poor to very good, respectively. Twenty taxa were identified (Figure 10), among which the most common are the long-ranging species *Coccolithus pelagicus* and *Reticulofenestra* small- and medium-sized.

Useful elements from a biostratigraphic point of view are represented by the presence of *Helicosphaera carteri*, common since early Miocene [61]; *Helicosphaera sellii* (Figure 11d), whose common occurrence marks the basal boundary of the Early Pliocene calcareous nannofossil zone MNN13 of [62]; and *Amaurolithus primus delicatus* (Figure 11e) and *A. delicatus* (Figure 11f), whose last occurrence falls within the lower part of the same biozone. Other significant species are *Ceratholithus acutus* (which postdates the Early Pliocene re-flooding of the Mediterranean Sea, following the Messinian Salinity Crisis [63,64]), and *Discoaster browveri*, *D. pentaradiatus* (Figure 11g,h), *D. surculus* (Figure 11a) and *D. subsurculus* (Figure 11b).

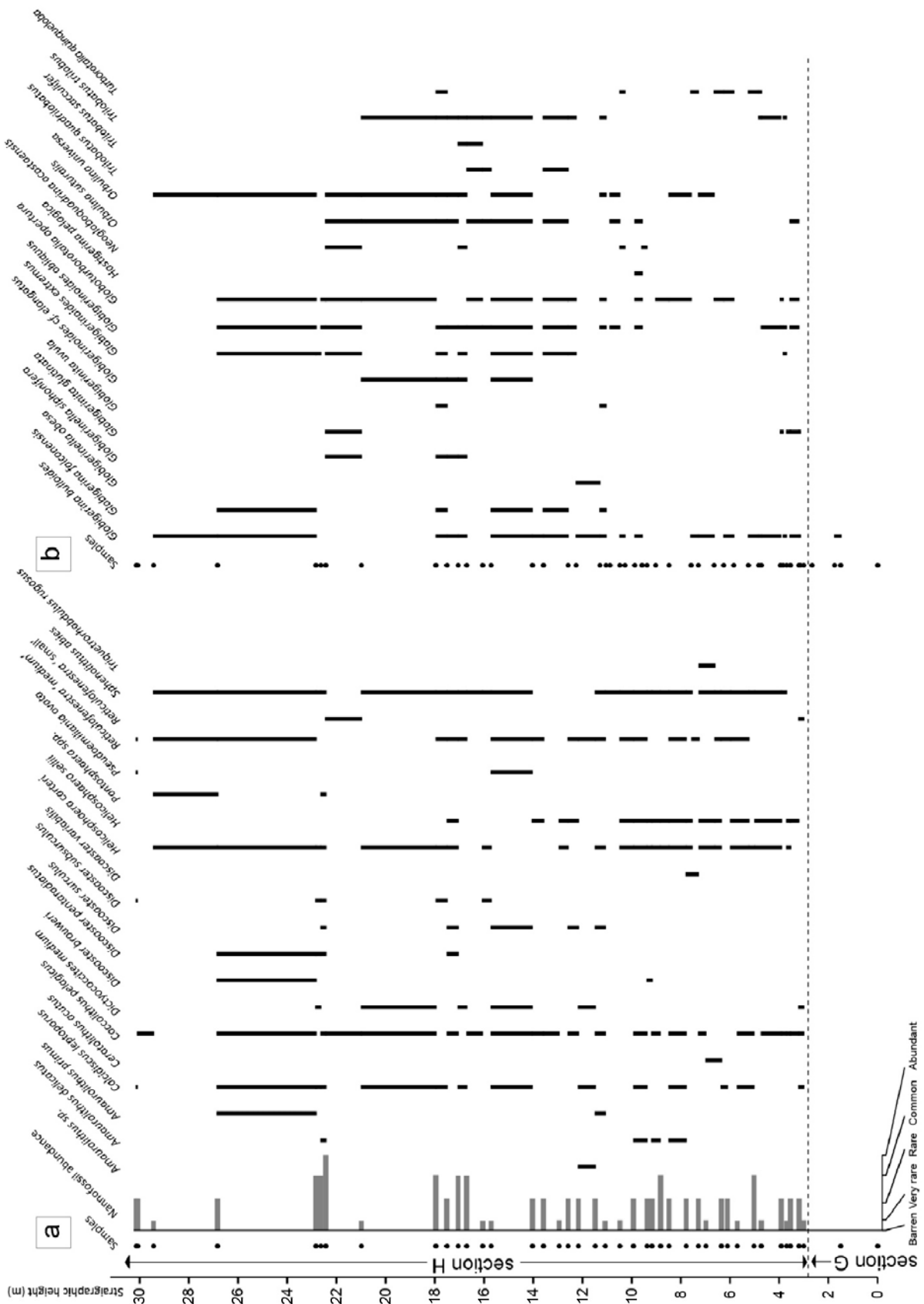


Figure 10. Stratigraphic distribution of (a) calcareous nannofossils and (b) planktonic Foraminifera in the Brunella composite section based on samples from sections G and H.

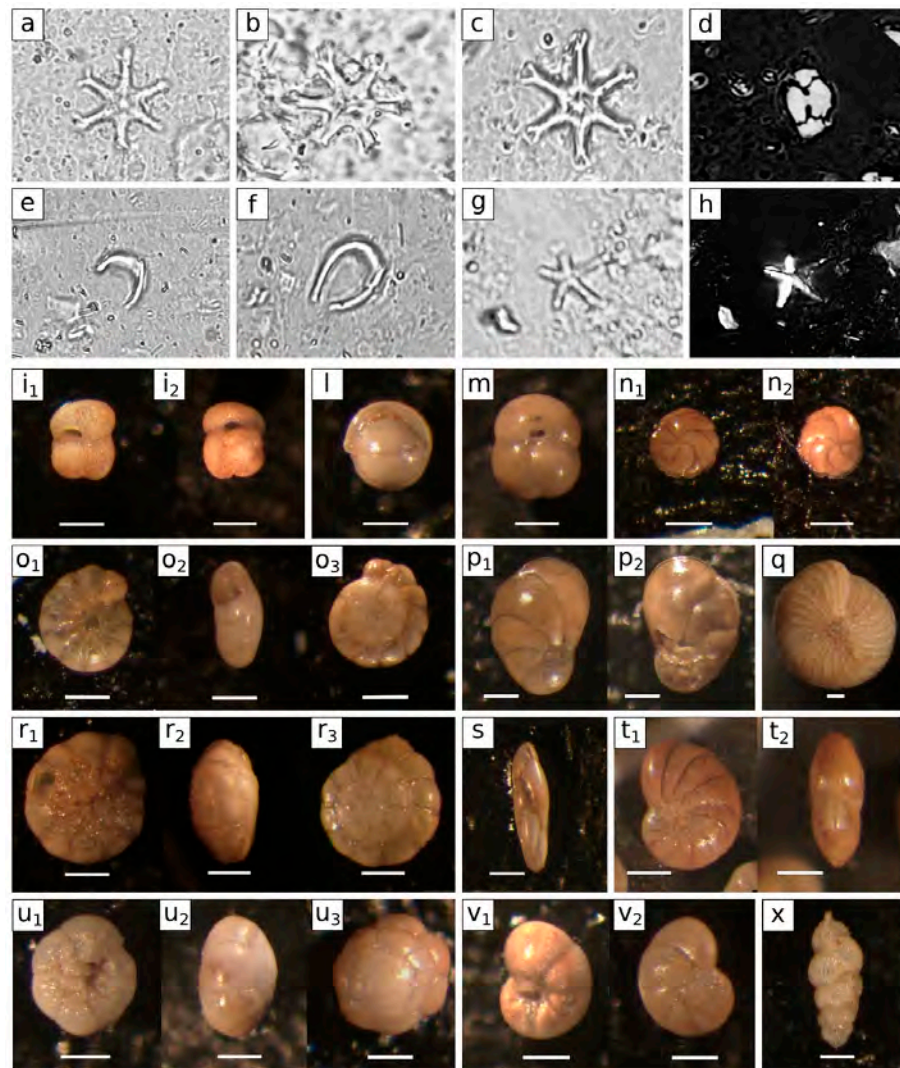


Figure 11. Microphoto of calcareous nannofossil (a–h; optical microscope 1000× magnification) and Foraminifera (i–x; scale bar 200 μm). (a) *Discoaster surculus* (// nicols, PM68); (b) *Discoaster subsurculus* (// nicols, PM68); (c) *Discoaster variabilis* (// nicols, PM28); (d) *Helicosphaera sellii* (X nicols, PM63); (e) *Amaurolithus primus* (// nicols, PM66); (f) *Amaurolithus delicatus* (// nicols, sample PM68); (g) *Discoaster pentaradiatus* (// nicols, PM67); (h) *Discoaster pentaradiatus* (X nicols; PM67). (i) *Globigerinoides cf. elongatus* (PM 64, 1—umbilical and 2—spiral view); (l) *Pullenia bulloides* (PM 52, apertural view); (m) *Sphaeroidina bulloides* (PM 52, umbilical view); (n) *Cassidulina neocarinata* (PM60, 1-apertural/side view and 2-side view); (o,r) *Ammonia beccarii* (PM 75, 1—umbilical, 2—apertural and 3—spiral view); (p) *Cancris auriculus* (PM59, 1—spiral and 2—umbilical view); (q) *Elphidium crispum* (PM76, side view); (s) *Fursenkoina schraebersiana* (PM59, side view); (t) *Nonion boueanum* (PM 03, 1-side and 2-apertural view); (u) *Ammonia inflata* (PM59, 1—umbilical, 2—peripheral and 3—spiral view); (v) *Valvulineria bradyana* (PM59, 1—umbilical and 2—spiral view); (x) *Uvigerina pygmaea* (PM59, side view).

Planktonic Foraminifera are generally rare and do not include any zonal marker. Nonetheless, it was possible to identify eighteen species (Figure 10b), among which the most frequent taxa are *Globigerina bulloides*, *G. falconensis*, *Globigerinoides cf. elongates* (Figure 11i), *G. extremus*, *G. obliquus*, *Globoturborotalita apertura*, *Orbulina suturalis*, *O. uniuersa* and *Trilobatus trilobus*.

4.3.2. Benthic Foraminifera

Apart from the Upper Miocene lowermost part of section G (Figure 3c), which is barren, benthic Foraminifera are generally very abundant in the Brunella composite section.

The stratigraphic distribution and abundance (estimated semi-quantitatively following [65]) of the most significant taxa (out of a total of 120 recognised species) is shown in Figure 12a,b. Abundant and stratigraphically ubiquitous taxa are *Ammonia beccarii* (Figure 11o,r), *A. inflata* (Figure 11u), *Bolivina* spp., *Bulimina* spp., *Fursenkoina schraebersiana* (Figure 11s), *Globobulimina* spp., *Nonion boueanum* (Figure 11t), *Pullenia bulloides* (Figure 11l), *Textularia* spp. and *Valvulineria bradyana* (Figure 11v). Based on benthic Foraminifera assemblages, four biofacies can be recognised, labelled 1 to 4 from bottom to top of the composite section (Figure 12a,b).

Biofacies 1 is typified by a very low specific diversity, dominated by *A. beccarii*, *Asterigerinata planorbis* and *Elphidium crispum* (Figure 11q), and occurs in the lowermost and coarser-grained marine part of the composite section (uppermost part of section G). On the other hand, Biofacies 2 (lowermost c. 8 metres of section H) characterises the fossiliferous marker bedset and the deposits immediately below and above and includes common to abundant *A. inflata*, *Bolivina* spp., *N. boueanum*, *Textularia* spp. and *V. bradyana* and common *Prosononion granosum* and *Sphaeroidina bulloides* (Figure 11m). Up-section (above c. 11 m), in parallel with the fining-upward of the succession, Biofacies 2 is replaced by Biofacies 3. The washing residues of samples from this interval show relatively lower terrigenous contents and a larger number of benthic Foraminifera compared to Biofacies 1 and 2. The assemblage is dominated by *A. inflata*, *Bolivina* spp., *Bulimina* spp., *Cassidulina neocarinata* (Figure 11n), *F. schraebersiana*, *Globobulimina* spp., *Heterolepa* spp., *N. boueanum*, *Pullenia bulloides*, *Textularia* spp. and *V. bradyana* (Figure 11v) and appear overall well-diversified. Finally, the sudden increase in terrigenous content of the washing residues in the uppermost part of the studied section is accompanied by establishment of Biofacies 4, which comprises abundant *N. boueanum*, common *A. beccarii*, and rare to common *Bolivina* spp. and *Bulimina* spp. (Figure 12a).

The micropalaeontological assemblage characterising the fossiliferous bedset in section W (Figure 3c) is typified by a very low planktonic foraminifera content and abundant benthic content (Figure 12b). This comprises *Ammonia beccarii*, *Criboelphidium decipiens*, *Elphidium macellum*, *Heterolepa* spp., *Nonion boueanum*, *Prosononion granosum* and *Reussella spinulosa*, and shows similarities to Biofacies 2 of section H (Figure 12a).

All in all, the composition of Biofacies 1–4, in tandem with plankton–benthos ratios always less than 3% [66], suggest a marine inner shelf depositional environment [67].

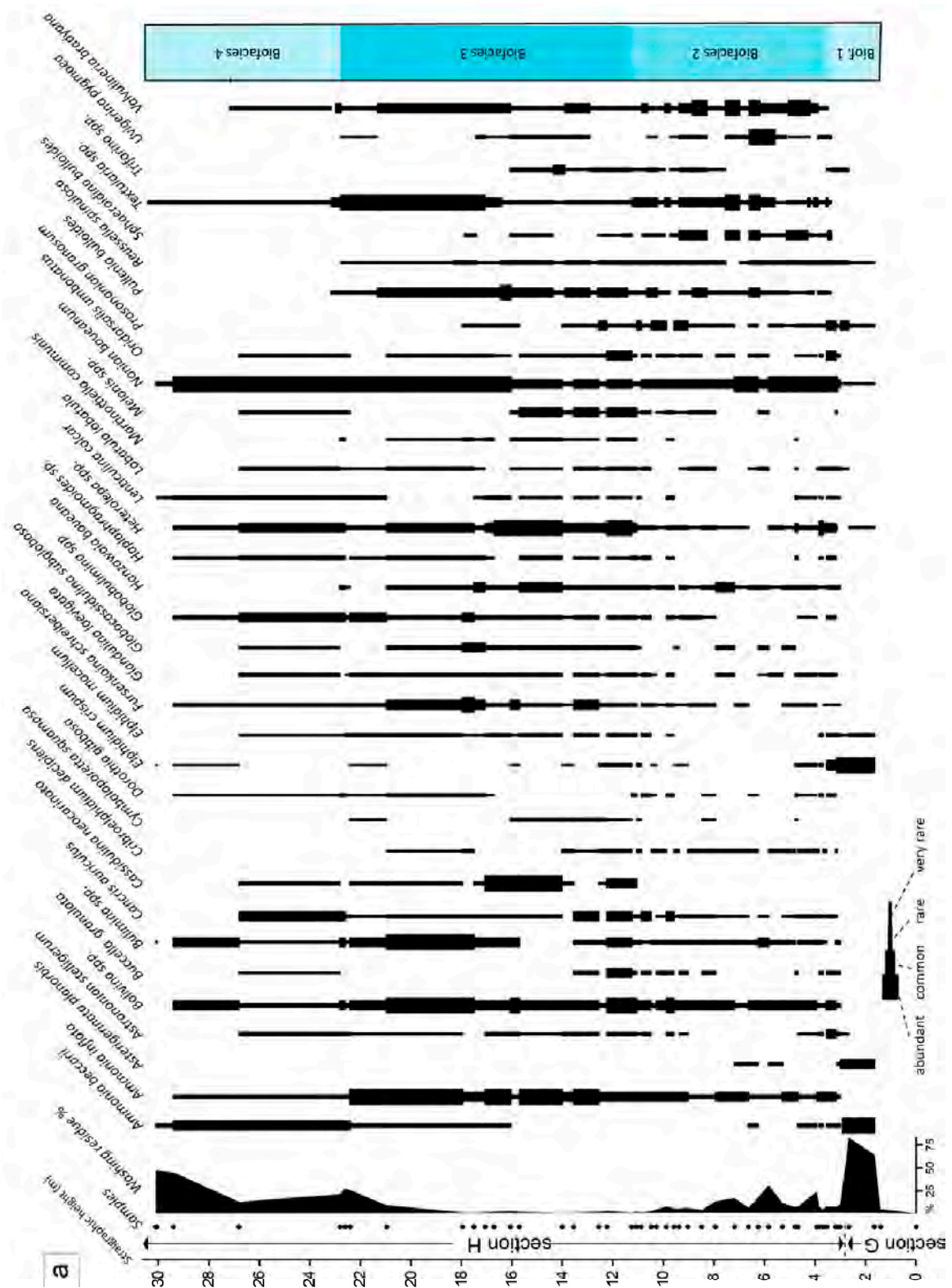


Figure 12. Cont.

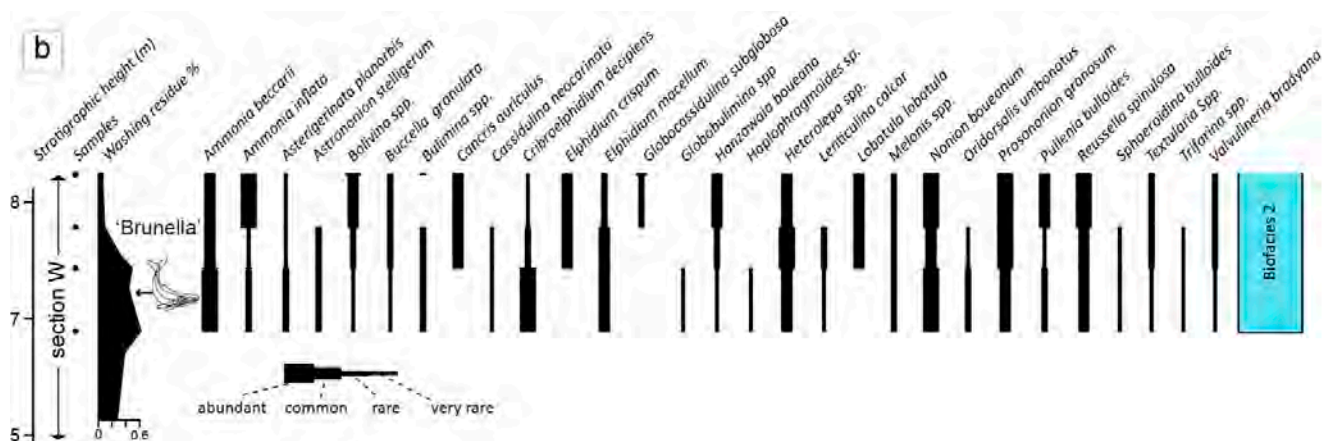


Figure 12. Spindle diagrams illustrating the stratigraphic distribution and estimated abundance of the most significant benthic Foraminifera species in (a) the investigated stratigraphy (sections G and H) and (b) the deposits embedding *Brunella* (section W).

5. Discussion

5.1. Depositional Age of *Brunella*

To date, the chronological assessment of Mediterranean fossil mysticetes indicates a poorly diversified Zanclean fauna with a generally ill-defined depositional age. The Zanclean mysticete fauna of Italy comprises a few Balaenopteridae and Balaenidae taxa whose age was inferred based on lithostratigraphy. These include the balaenopterids *Archaeobalaenoptera castriarquati* and *Cetotheriophanes capellini*, and *C. cortesii* from Emilia Romagna [13], unearthed from sedimentary rocks with likely ages in the ranges 4.12–3.84 Ma and 5.33–3.57 Ma, respectively, and the balaenid *Balaena montalionis* from Tuscany, with a supposed age between 4.5 and 3.9 Ma [68].

The discovery of *Brunella* [15,33–35] was important in that it added a specimen to the existing database of Early Pliocene balaenopterids, which based on a preliminary anatomical assessment of selected bones (i.e., mandibular, ear and squamosal bones; [16]) appears remarkably different from *Cetotheriophanes* and *Archaeobalaenoptera*. Therefore, dating *Brunella* is key to better understanding of the Neogene mysticetes phylogenesis.

Even if calcareous plankton is generally rare in the *Brunella* composite section, calcareous nannofossils and Foraminifera assemblages (see Section 4.3) provide useful biostratigraphic insights. Key biostratigraphic elements of the calcareous nannofossil assemblage is the concomitant presence of *Ceratholithus acutus*, which postdates the Messinian Salinity Crisis [63,64]; *Helicosphaera sellii*, whose common occurrence marks the basal boundary of the Early Pliocene calcareous nannofossil zone MNN13 of [62]; and *Amaurolithus primus* and *A. delicatus*, whose last occurrence falls within the lower part of the same nannofossil biozone (Figure 13). Despite the lack of zonal markers in the planktonic Foraminifera assemblage, the presence of *Globigerinoides cf. elongatus* and the concomitant absence of typical specimens of *G. elongatus* suggest that the sampled interval was deposited before the first occurrence of *Globorotalia puncticulata* [69], corresponding to the basal boundary of the Early Pliocene MPI3 Biozone of [70] (Figure 13).

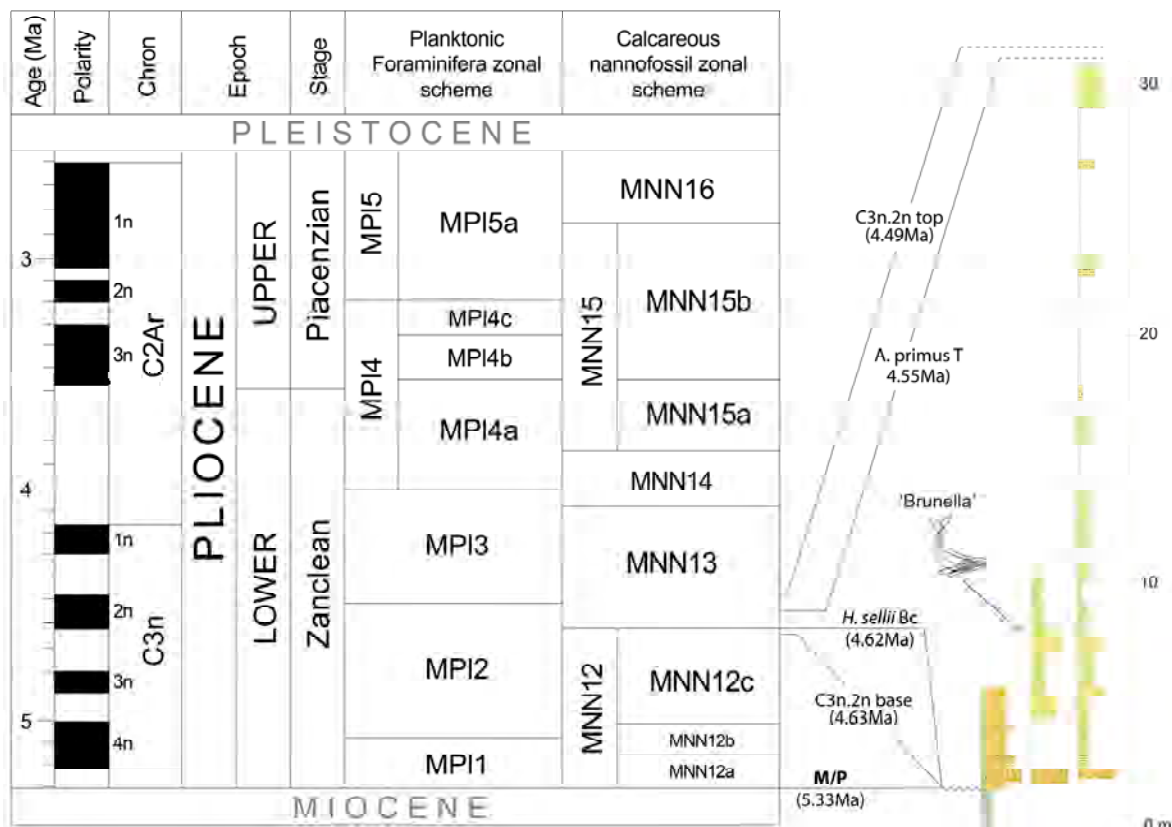


Figure 13. Bio-magneto-chronostratigraphic framework of the Brunella Composite section. Planktonic Foraminifera and calcareous nannofossil zonal schemes are from [70] and [62], respectively. The geological time scale (GTS) is from [71], following the ATNTS2004/2012 by [39,72].

On the other hand, palaeomagnetic data (Section 4.2) show that the isolated ChRM component directions are the product of primary (sedimentary) remanent magnetisation and that the marine part of the Brunella composite section was deposited during a normal polarity chron. Specifically, rock magnetism experiments, ChRM unblocking temperatures and the magnetic directions allow excluding that the remanent magnetisation was acquired either during a late diagenesis (e.g., due to growth of authigenic greigite; [73]) or as the product of modern weathering (i.e., at any time after the local tectonic rotation highlighted by mean declination; Figure 8 and Table 1).

All in all, the magnetobiochronology results of this work indicate that the marine part of the Brunella composite section was deposited during a normal polarity time interval after the first common occurrence of the calcareous nannofossil *Helicosphaera sellii*, and before the first occurrence of the planktonic foraminifer *Globorotalia puncticulata* and the last occurrence of the calcareous nannofossils *Amaurolithus primus* and *A. delicatus*. This corresponds to the interval of the polarity Chron C3n.2n between 4.62 Ma (*H. sellii* Bc—Base common) and 4.55 Ma (*A. primus* T—Top) (Figure 13) and the lowermost part of the calcareous nannofossil zone MNN13 of [62]. These results place the depositional age of Brunella within a very short chronological interval of c. 70 Ky and suggest that, in agreement with previous estimations by [74], the investigated sedimentary section was deposited at a pace greater than c. 40 cm/Ky.

5.2. Palaeoenvironmental Insights from Sedimentary Facies, AMS and Benthic Foraminifera

Even though the depositional environment of the Lower Pliocene cropping out at Poggio alle Mura is discussed in a number of works [1,37,42], sedimentary facies of the deposits embedding Brunella and their significance have never been investigated in detail.

Stratigraphic position (i.e., above continental Late Miocene deposits) and sedimentary character (e.g., grain-size, texture, sharp top, macro-fossiliferous content, etc.; see Section 4.1) of the basal conglomerate that initiates the fining-upward marine part of the Brunella composite section, suggests it may represent a winnowing lag associated to a wave-ravinement surface [50–53] formed during the Early Pliocene regional transgression [75]. In keeping with this interpretation, the benthic Foraminifera assemblage from this lag deposit (Biofacies 1) is characterised by the *Ammonia–Elphidium* assemblages (Section 4.3.2), typical in mobile sediments from highly energetic shallow water settings [76–78].

The fossiliferous bedset that hosted Brunella lays immediately above this basal lag. It is relatively sandy and rich in mollusc shell fragments, locally bioturbated, and typified by a relatively more diversified benthic Foraminifera assemblage (Biofacies 2) suggestive of an energetic habitat, albeit deeper than that of Biofacies 1. Sedimentary facies and thickness of this bedset are laterally highly variable (Figure 3c), becoming relatively coarser and fossiliferous toward the west as the bedset thickens. This stark facies and thickness lateral variability can be interpreted to reflect deposition onto an uneven seafloor affected by wave action. Continuous sediment reworking by wave action is confirmed by the scrutiny of AMS data from section H (Section 4.2.3). In fact, AMS highlights a highly dispersed magnetic fabric that is hardly interpretable as the result suspension settling plus traction (by a slow-moving unidirectional current) in a low-energy environment [60]. These observations, together with the disarticulated nature of the partial skeleton of Brunella, indicate deposition in a nearshore setting above the fair-weather base level.

6. Conclusions

This contribution focusses on age and depositional environment of a c. 31 m thick section straddling the fossil find of an Early Pliocene baleen whale Brunella from the sedimentary fill of the Middle Ombrone Basin of Tuscany. Age and depositional environment of Brunella have been addressed earlier, but never with an integrated magnetobiostratigraphic approach.

Integration of sedimentary facies, palaeomagnetism and micropalaeontological (Foraminifera and calcareous nannofossils) analyses allows drawing the following conclusions:

- Magnetobiochronology results provide evidence that the clastic sediments embedding Brunella were deposited during the polarity Chron C3n.2n and between 4.62 Ma (*H. sellii* Bc—Base common) and 4.55 Ma (*A. primus* T—Top), which corresponds to the lowermost part of the calcareous nannofossil MNN13 zone;
- The depositional age of the marine interval of the investigated composite section is constrained to be within a very short chronological interval (c. 70 Ky) of the Zanclean, which makes Brunella the earliest baleen whale of Tuscany postdating the Messinian Salinity Crisis;
- Sedimentary facies and benthic Foraminifera assemblages indicate Brunella was buried by sediments accumulating in a nearshore setting above the fair-weather base level, at a pace greater than c. 40 cm/Ky.

Author Contributions: Conceptualisation, M.M., L.M.F. and I.M.; methodology, M.M., L.M.F., I.M., A.D.S. and G.M.; software, M.M.; validation, M.M., L.M.F., I.M. and G.M.; formal analysis, M.M., L.M.F., I.M., V.B., A.D.S. and G.M.; investigation, M.M., L.M.F. and I.M.; resources, M.M.; data curation, M.M., L.M.F. and I.M.; writing—original draft preparation, M.M., L.M.F., I.M., M.B. and G.M.; writing—review and editing, M.M., L.M.F., I.M., M.B. and G.M.; visualisation, M.M.; supervision, L.M.F.; project administration, L.M.F.; funding acquisition, M.M., L.M.F. and M.B. All authors have read and agreed to the published version of the manuscript.

Funding: Palaeomagnetic data collection and laboratory work was funded by FONDAZIONE BANFI, grant ‘RICERCA 2020-2021’.

Institutional Review Board Statement: Not applicable.

Informed Consent Statement: Not applicable.

Data Availability Statement: Not applicable.

Acknowledgments: The Brunella project was promoted by Soprintendenza Archeologia, Belle Arti e Paesaggio per le province di Siena, Grosseto and Arezzo and supported by Fondazione Banfi and Banfi Società agricola S.r.l. M.M. wishes to thank Francesca Cifelli (Università degli Studi Roma 3) for AMS acquisition.

Conflicts of Interest: The authors declare no conflict of interest. The funders had no role in the design of the study; in the collection, analyses, or interpretation of data; in the writing of the manuscript; or in the decision to publish the results.

References

1. Dominici, S.; Danise, S.; Benvenuti, M. Pliocene stratigraphic paleobiology in Tuscany and the fossil record of marine megafauna. *Earth-Sci. Rev.* **2018**, *176*, 277–310. [[CrossRef](#)]
2. Bisconti, M. Cenozoic environmental changes and evolution of baleen whales. In *Whales and Dolphins: Behavior, Biology and Distribution*; Murray, C.A., Ed.; Nova Publishing: New York, NY, USA, 2010; pp. 1–46.
3. Bisconti, M. Storia evolutiva dei Mysticeti: Diversità, estinzioni e conservazione. In *Estinzioni di Massa e Biodiversità—XXII Giornata dell'Ambiente*; Battaglia, B., Bullini, L., D'Argenio, B., Gerola, F.M., Pignatti, S., Scarascia Mugnozza, G.T., Eds.; Accademia Nazionale dei Lincei, Atti dei Convegni Lincei, Bardi Editore: Roma, Italy, 2005; Volume 220, pp. 95–105.
4. Hsü, K.J.; Ryan, W.B.F.; Cita, M.B. Late Miocene desiccation of the Mediterranean. *Nature* **1973**, *242*, 240–244. [[CrossRef](#)]
5. Bisconti, M.; Munsterman, D.K.; Post, K. A new balaenopterid whale from the late Miocene of the Southern North Sea Basin and the evolution of balaenopterid diversity (Cetacea, Mysticeti). *PeerJ* **2019**, *7*, e6915. [[CrossRef](#)] [[PubMed](#)]
6. Whitmore, F.C., Jr. Neogene climatic change and the emergence of the modern whale fauna of the North Atlantic Ocean. In *Contributions in Marine Mammal Paleontology Honoring Frank C. Whitmore*; Berta, A., Deméré, T.A., Eds.; Proceedings of the San Diego Society of Natural History San Diego; San Diego Society of Natural History: San Diego, CA, USA, 1994; Volume 29, pp. 223–227.
7. Bisconti, M. Evolutionary history of Balaenidae. *Cranium* **2003**, *20*, 9–50.
8. Bisconti, M. Taxonomy and evolution of the Italian Pliocene Mysticeti (Mammalia, Cetacea): A state of the art. *Boll. Soc. Paleont. Ital.* **2009**, *48*, 147–156.
9. Dominici, S.; Danise, S.; Cau, S.; Freschi, A. The awkward record of fossil whales. *Earth-Sci. Rev.* **2019**, *205*, 103057. [[CrossRef](#)]
10. Bisconti, M.; Pellegrino, L.; Carnevale, G. Evolution of gigantism in right and bowhead whales (Cetacea, Mysticeti, Balaenidae). *Biol. J. Linn. Soc.* **2021**, *134*, 498–524. [[CrossRef](#)]
11. Bisconti, M.; Bosselaers, M. On Plesiocetus Van Beneden, 1859 (Mammalia, Cetacea, Mysticeti). *Riv. Ital. Paleontol. Stratigr.* **2021**, *127*, 231–274. [[CrossRef](#)]
12. Bisconti, M. New description, character analysis and preliminary phylogenetic assessment of two Balaenidae skulls from the Italian Pliocene. *Palaeontogr. Ital.* **2000**, *87*, 37–66.
13. Cau, S.; Freschi, A. Revisione cronostatigrafica dei cetacei del Plio-Pleistocene nell'Appennino settentrionale. *Parva Nat.* **2020**, *15*, 59–83.
14. Foresi, L.M.; Bambini, A.M. Il Neogene. In *Atlante dei Dati Biostratigrafici della Toscana*; Cerrina Feroni, A., Ed.; CNR-IGG: Pisa, Italy, 2010.
15. Scotton, R.; Bigazzi, R.; D'Amore, G.; Di Marco, S.; Koenig, E.; Nannini, P.; Santagati, P.; Tabolli, J.; Tartarelli, G.; Tarantini, M.; et al. Il Progetto "Brunella": Principali attività preparatorie e strategie di comunicazione intorno ad un balenoteride pliocenico in Toscana. *Parva Nat.* **2020**, *15*, 85–133.
16. Bisconti, M.; Scotton, R.; Santagati, P.; Foresi, L.M.; Ragaini, L.; Tartarelli, G.; Carnevale, G.; Buckeridge, J.; Koenig, E.; Tabolli, J.; et al. A Whale in a Vineyard: Palaeontological Preparation and Education During the 'Brunella' Project, a Large-Scale Conservation Effort Focused on a Pliocene Whale in Southern Tuscany, Italy. *Geoheritage* **2023**, *15*, 1–19. [[CrossRef](#)]
17. Damiani, A.V.; Gandin, A.; Pannuzzi, L. Il Bacino dell'Ombrone-Orcia nelquadro dell'evoluzione paleografica e tettonica della Toscana meridionale. *Mem. Soc. Geol. Ital.* **1981**, *21*, 281–287.
18. Bossio, A.; Costantini, A.; Foresi, L.M.; Mazzei, R.; Monteforti, B.; Salvatorini, G.; Sandrelli, F. Notizie preliminari sul Pliocene del bacino del medio Ombrone e della zona di Roccastrada. *Atti Soc. Toscana Sci. Nat.* **1991**, *98*, 259–269.
19. Bossio, A.; Costantini, A.; Foresi, L.M.; Mazzei, R.; Monteforti, B.; Radi, L.; Salvatorini, G.; Sandrelli, F. *Carta Geologica dell'Area del Medio Ombrone (Province di Siena e Grosseto)*; Cartografia S.E.L.C.A.: Firenze, Italy, 1991.
20. Benvenuti, M.; Moratti, G.; Sani, F.; Bonini, M.; Oms, O.L.; Papini, M.; Rook, L.; Cavallina, C.; Cavini, L. Messinian-earliest Zanclean tectonic-depositional dynamics of the Cinigiano-Baccinello and Velona basins (Tuscany, Italy). *Ital. J. Geosci.* **2015**, *134*, 237–254. [[CrossRef](#)]
21. Bossio, A.; Cerri, R.; Costantini, A.; Gandin, A.; Lazzarotto, A.; Magi, M.; Sandrelli, F. I Bacini distensivi Neogenici e Quaternari della Toscana. In *76° Riunione Estiva della Società Geologica Italiana—Convegno SIMP*; Guida all'Escursione: Firenze, Italy, 1992; Volume B4, pp. 198–227.
22. Bossio, A.; Costantini, A.; Lazzarotto, A.; Liotta, D.; Mazzanti, R.; Mazzei, R.; Salvatorini, G.; Sandrelli, F. Rassegna delle conoscenze sulla stratigrafia del neautoctono toscano. *Mem. Soc. Geol. Ital.* **1993**, *49*, 17–98.

23. Martini, I.P.; Sagri, M. Tectono-sedimentary characteristics of Late Miocene-Quaternary extensional basins of the Northern Apennines, Italy. *Earth Sci. Rev.* **1993**, *34*, 197–233. [[CrossRef](#)]
24. DeCelles, P.G. Foreland basin systems revisited: Variations in response to tectonic settings. In *Tectonics of Sedimentary Basins: Recent Advances*; Busby, C., Azor, A., Eds.; Wiley-Blackwell: Hoboken, NJ, USA, 2012; pp. 405–426.
25. Martini, I.; Ambrosetti, E.; Brogi, A.; Aldinucci, M.; Zwaan, F.; Sandrelli, F. Polyphase extensional basins: Interplay between tectonics and sedimentation in the Neogene Siena-Radicofani Basin (Northern Apennines, Italy). *Int. J. Earth Sci.* **2021**, *110*, 1729–1751. [[CrossRef](#)]
26. Pascucci, V.; Costantini, A.; Martini, I.P.; Dringoli, R. Tectonosedimentary analysis of a complex, extensional, Neogene basin formed on thrust-faulted, Northern Apennines hinterland: Radicofani Basin, Italy. *Sediment. Geol.* **2006**, *183*, 71–97. [[CrossRef](#)]
27. Mattei, M.; Kissel, C.; Funicello, R. No tectonic rotation of the Tuscan Tyrrhenian margin (Italy) since late Messinian. *J. Geophys. Res. Solid Earth* **1996**, *101*, 2835–2845. [[CrossRef](#)]
28. Benvenuti, M.; Del Conte, S.; Scarselli, N.; Dominici, S. Hinterland basin development and infilling through tectonic and eustatic processes: Latest Messinian-Gelasian Valdelsa Basin, Northern Apennines, Italy. *Basin Res.* **2014**, *26*, 387–402. [[CrossRef](#)]
29. Bonini, M.; Sani, F.; Stucchi, E.M.; Moratti, G.; Benvenuti, M.; Menanno, G.; Tanini, C. Late Miocene shortening of the Northern Apennines back-arc. *J. Geodyn.* **2014**, *74*, 1–31. [[CrossRef](#)]
30. Brogi, A. Bowl-shaped basin related to low-angle detachment during continental extension: The case of the controversial Neogene Siena Basin (central Italy, Northern Apennines). *Tectonophysics* **2011**, *499*, 54–76. [[CrossRef](#)]
31. Brogi, A. Late evolution of the inner Northern Apennines from the structure of the Monti del Chianti-Monte Cetona ridge (Tuscany, Italy). *J. Struct. Geol.* **2020**, *141*, 104205. [[CrossRef](#)]
32. Regione Toscana. Geological Maps at Scale 1:10,000 Composing the Sheet n. 287 (scale 1:50,000) Montevarchi. 2007. Available online: <http://www.regione.toscana.it/ambienteeterritorio/geologia/index.html> (accessed on 1 February 2023).
33. De Pretis, F. *La Balena che Nuotava nel Mediterraneo Nano. 3 Domande a Michelangelo Bisconti*; La Stampa TuttoScienze: Torino, Italy, 2017; p. 7.
34. Batini, G. *La Toscana delle Balene*; Edizioni Polistampa: Firenze, Italy, 2009. Available online: <https://www.ibs.it/toscana-delle-balene-quando-grandi-libro-giorgio-batini/e/9788859605010> (accessed on 1 February 2023).
35. Scotton, R.; Bigazzi, R.; Casati, S.; D'Amore, G.; Di Marco, S.; Foresi, L.M.; Koenig, E.; Ragaini, L.; Tabolli, J.; Tarantini, M.; et al. The “Brunella” Project: Preparation and study of a mysticete from the Early Pliocene of Tuscany. *Fossilia* **2018**, *15*, 61–63.
36. Motta, S. *Note Illustrative della Carta Geologica d'Italia alla Scala 1:100,000*; Foglio 128 Grosseto: Ercolano, Italy, 1969.
37. Tinelli, C. Marine Vertebrates from Pliocene Shell Beds from Tuscany (Italy): Prospecting, Taphonomy, Palaeoecology and Systematic Palaeontology. Ph.D. Thesis, Università di Pisa, Pisa, Italy, 2013.
38. Sprovieri, R. Mediterranean Pliocene biochronology: An high resolution record based on quantitative planktonic foraminifera distribution. *Riv. Ital. Paleontol. Stratigr.* **1992**, *98*, 61–100.
39. Hilgen, F.; Lourens, L.J.; Van Dam, J.A.; Beu, A.G.; Boyes, A.F.; Cooper, R.A.; Krigsman, W.; Ogg, J.G.; Piller, W.E.; Wilson, D.S. The Neogene period. In *The Geologic Time Scale 2012*; Gradstein, F.M., Ogg, J.G., Schmitz, M., Ogg, G., Eds.; Elsevier Publ.: Amsterdam, The Netherlands, 2012; pp. 923–978.
40. Tinelli, C.; Ribolini, A.; Bianucci, G.; Bini, M.; Landini, W. Ground penetrating radar and palaeontology: The detection of sirenian fossil bones under a sunflower field in Tuscany (Italy). *Comptes Rendus Palevol* **2012**, *11*, 445–454. [[CrossRef](#)]
41. Sorbi, S.; Vaiani, S.C. New sirenian record from Lower Pliocene sediments of Tuscany (Italy). *Riv. Ital. Paleontol. Stratigr.* **2007**, *113*, 299–304.
42. Dominici, S.; Forli, M. Lower Pliocene molluscs from southern Tuscany (Italy). *Boll. Soc. Pal. Ital.* **2021**, *60*, 69–98.
43. Lowrie, W. Identification of ferromagnetic minerals in a rock by coercivity and unblocking temperature properties. *Geophys. Res. Lett.* **1990**, *17*, 159–162. [[CrossRef](#)]
44. Hrouda, F. Magnetic anisotropy of rocks and its application in geology and geophysics. *Geophys. Surv.* **1982**, *5*, 37–82. [[CrossRef](#)]
45. Tarling, D.H.; Hrouda, F. *The Magnetic Anisotropy of Rocks*; Chapman & Hall: London, UK, 1993; 217p.
46. Hrouda, F.; Janak, F. The changes in shape of the magnetic susceptibility ellipsoid during progressive metamorphism and deformation. *Tectonophysics* **1976**, *34*, 135–148. [[CrossRef](#)]
47. Kraus, M.J.; Aslan, A. Eocene hydromorphic paleosols: Significance for interpreting ancient floodplain processes. *J. Sed. Petrol.* **1993**, *63*, 453–463.
48. Mancini, M.; Marini, M.; Moscatelli, M.; Stigliano, F.; Cavinato, G.P.; Di Salvo, C.; Simionato, M. Stratigraphy of the Palatine hill (Rome, Italy): A record of repeated middle pleistocene-holocene paleovalley incision and infill. *Alp. Mediterr. Quat.* **2018**, *31*, 171–194.
49. Nummendal, D.; Swift, D.J.P. *Transgressive Stratigraphy at Sequence-Bounding Unconformities: Some Principles Derived from Holocene and Cretaceous Examples*; SEPM Special Publication: Tulsa, OK, USA, 1987; Volume 41, pp. 241–260.
50. Siggerud, E.I.H.; Steel, R.J.; Pollard, J.E. Bored pebbles and ravinement surface clusters in a transgressive systems tract, Sant Llorenç del Munt fan-delta complex, SE Ebro Basin, Spain. *Sediment. Geol.* **2000**, *138*, 161–177. [[CrossRef](#)]
51. Hwang, I.G.; Heller, P.L. Anatomy of a transgressive lag: Panther Tongue Sandstone, Star Point Formation, central Utah. *Sedimentology* **2002**, *49*, 977–999. [[CrossRef](#)]
52. Cattaneo, A.; Steel, R.J. Transgressive deposits: A review of their variability. *Earth-Sci. Rev.* **2003**, *62*, 187–228. [[CrossRef](#)]

53. Ambrosetti, E.; Martini, I.; Sandrelli, F. Shoal-water deltas in high-accommodation settings: Insights from the lacustrine Valimi Formation (Gulf of Corinth, Greece). *Sedimentology* **2017**, *64*, 425–452. [[CrossRef](#)]
54. Colomera, L.; Mountney, N.P. On the geological significance of clastic parasequences. *Earth-Sci. Rev.* **2020**, *201*, 103062. [[CrossRef](#)]
55. Tauxe, L.; Mullender, T.A.T.; Pick, T. Potbellies, wasp-waists, and superparamagnetism in magnetic hysteresis. *J. Geophys. Res. Solid Earth* **1996**, *101*, 571–583. [[CrossRef](#)]
56. Tauxe, L.; Bertram, H.N.; Seberino, C. Physical interpretation of hysteresis loops: Micromagnetic modeling of fine particle magnetite. *Geochem. Geophys. Geosyst.* **2002**, *3*, 1–22. [[CrossRef](#)]
57. Day, R.; Fuller, M.; Schmidt, V.A. Hysteresis properties of titanomagnetites: Grain-size and compositional dependence. *Phys. Earth Planet. Int.* **1977**, *13*, 260–267. [[CrossRef](#)]
58. Dunlop, D.J. Theory and application of the Day plot (Mrs/Ms versus Hcr/Hc) 1. Theoretical curves and tests using titanomagnetite data. *J. Geophys. Res.* **2002**, *107*, 1–22.
59. Roberts, A.P.; Chang, L.; Rowan, C.J.; Horng, C.S.; Florindo, F. Magnetic properties of sedimentary greigite (Fe₃S₄): An update. *Rev. Geophys.* **2011**, *49*, RG1002. [[CrossRef](#)]
60. Tauxe, L.; Banerjee, S.K.; Butler, R.F.; van der Voo, R. *Essentials of Paleomagnetism*. 5th Web Edition. 2018. Available online: <https://earthref.org/MagIC/books/Tauxe/Essentials/> (accessed on 13 February 2023).
61. Fabbrini, A.; Baldassini, N.; Caricchi, C.; Foresi, L.M.; Sagnotti, L.; Dinarés-Turell, J.; Di Stefano, A.; Lirer, F.; Menichetti, M.; Winkler, A.; et al. In search of the Burdigalian GSSP: New evidence from the Contessa Section (Italy). *Ital. J. Geosci.* **2019**, *138*, 274–295. [[CrossRef](#)]
62. Di Stefano, A.; Baldassini, N.; Raffi, I.; Fornaciari, E.; Incarbona, A.; Negri, A.; Bonomo, S.; Villa, G.; Di Stefano, E.; Rio, D. Neogene-Quaternary Mediterranean Calcareous Nannofossil Biozonation and Biochronology. *Stratigraphy* **2023**, *in press*.
63. Iaccarino, S.; Castradori, D.; Cita, M.B.; Di Stefano, E.; Gaboardi, S.; McKenzie, J.A.; Spezzaferri, S.; Sprovieri, R. The Miocene/Pliocene boundary and the significance of the earliest Pliocene flooding in the Mediterranean. *Mem. Soc. Geol. Ital.* **1999**, *54*, 109–131.
64. Maniscalco, R.; Casciano, C.I.; Distefano, S.; Grossi, F.; Di Stefano, A. Facies analysis in the Second Cycle Messinian evaporites predating the early Pliocene reflooding: The Balza Soletta section (Corvillo Basin, central Sicily). *Ital. J. Geosci.* **2019**, *138*, 301–316. [[CrossRef](#)]
65. Cita, M.B. *Micropaleontologia*; Cisalpino Goliardica: Milano, Italy, 1983.
66. Van der Zwaan, G.J.; Jorissen, F.J.; De Stigter, H.C. The depth dependency of planktonic/benthic foraminiferal ratios: Constraints and applications. *Mar. Geol.* **1990**, *95*, 1–16. [[CrossRef](#)]
67. Murray, J.W. *Ecology and Applications of Benthic Foraminifera*; Cambridge University Press: New York, NY, USA, 2006; pp. 1–426.
68. Dominici, S.; Mazzanti, R.; Nencini, C. Geologia dei dintorni di San Miniato tra l’Arno, l’Elsa e l’Era. *Quaderni del Museo di Storia Naturale di Livorno* **1995**, *14* (Suppl. S1), 1–35.
69. Bossio, A.; Foresi, L.M.; Mazzanti, R.; Mazzei, R.; Salvatorini, G. Note micropaleontologiche sulla successione miocenica del Torrente Morra e su quella Pliocenica del Bacino dei Fiumi Tora e Fine (Province di Livorno e Pisa). *Atti Soc. Toscana Sci. Nat.* **1997**, *104*, 85–134.
70. Lirer, F.; Antonio, C.; Claudia, C.; Elena, T.; Francisco, S.; Salvatorini, G.; Turco, E.; Cosentino, C.; Sierro, F.J.; Caruso, A. Mediterranean Neogene planktonic foraminifer biozonation and biochronology. *Earth Sci. Rev.* **2019**, *196*, 102869. [[CrossRef](#)]
71. Raffi, I.; Wade, B.S.; Palike, H.; Beu, A.G.; Cooper, R.; Crundwell, M.P.; Krijgsman, W.; Moore, T.; Raine, I.; Sardella, R.; et al. The Neogene Period. In *The Geological Time Scale 2020*; Gradstein, F.M., Ogg, J.G., Schmitz, M.D., Ogg, G.M., Eds.; Elsevier: Amsterdam, The Netherlands, 2020; Volume 29, pp. 1141–1215.
72. Lourens, L.J.; Hilgen, F.J.; Shackleton, N.J.; Laskar, J.; Wilson, D. The Neogene Period. In *A Geologic Time Scale 2004*; Gradstein, F., Ed.; Cambridge University Press: Cambridge, UK, 2004; Volume 21, pp. 409–440.
73. Florindo, F.; Sagnotti, L. Palaeomagnetism and rock magnetism in the upper Pliocene Valle Ricca (Rome, Italy) section. *Geophys. J. Int.* **1995**, *123*, 340–354. [[CrossRef](#)]
74. Channel, J.E.T.; Poli, M.S.; Rio, D.; Sprovieri, R.; Villa, G. Magnetic stratigraphy and biostratigraphy of Pliocene “argille azzurre” (Northern Apennines, Italy). *Palaeogeogr. Palaeoclimatol. Palaeoecol.* **1994**, *110*, 83–102. [[CrossRef](#)]
75. Bossio, A.; Costantini, A.; Foresi, L.M.; Lazzarotto, A.; Mazzanti, R.; Mazzei, R.; Pascucci, V.; Salvatorini, G.; Sandrelli, F.; Terzuoli, A. Space-time sedimentary evolution of the Neogene-Quaternary sediments of the western side of the Northern Apennines (Italy). *Mem. Soc. Geol. Ital.* **1998**, *52*, 513–525.
76. Blanc-Vernet, L. Contribution à l’étude des Foraminifères de Méditerranée. *Rec. Trav. St. Mar. Endoume* **1969**, *48*, 5–281.
77. Jorissen, F.J. The distribution of benthic foraminifera in the Adriatic Sea. *Mar. Micropaleontol.* **1987**, *12*, 21–48. [[CrossRef](#)]
78. Sen Gupta, B.K. Foraminifera in marginal marine environments. In *Modern Foraminifera*; Sen Gupta, B.K., Ed.; Kluwer Academic Publishers: Dordrecht, The Netherlands, 2003; pp. 141–159.

Disclaimer/Publisher’s Note: The statements, opinions and data contained in all publications are solely those of the individual author(s) and contributor(s) and not of MDPI and/or the editor(s). MDPI and/or the editor(s) disclaim responsibility for any injury to people or property resulting from any ideas, methods, instructions or products referred to in the content.